6974–6982 *Nucleic Acids Research, 2018, Vol. 46, No. 14* *Published online 3 July 2018*
doi: 10.1093/nar/gky521

The role of spacer sequence in modulating turn-on fluorescence of DNA-templated silver nanoclusters

Yan Shan Ang, Wei Wen Elvin Woon and Lin-Yue Lanry Yung*

Department of Chemical & Biomolecular Engineering, National University of Singapore, 4 Engineering Drive 4, Singapore 117585

Received January 22, 2018; Revised May 18, 2018; Editorial Decision May 23, 2018; Accepted June 09, 2018

ABSTRACT

Guanine activation of fluorescence in DNA templated silver nanoclusters (AgNCs) is an interesting physical phenomenon which has yet to be fully understood to date. While the individual role of cytosine and guanine has been established, there is still a knowledge gap on how the AgNC–DNA system switches from dark to bright state. Here, we present evidence on the universal role of the DNA spacer sequence in physically separating two Ag^+-binding cytosine sites to maintain the dark state while holding them together for structural re-organization by the guanine-rich strand to activate the bright state. The extent of turn-on signal could be modulated by adjusting the spacer length and composition. The ATATA spacer sequence was found to have negligible dark state fluorescence and a turn-on effect of 2440-fold, which was almost five times of the highest factor reported to date.

INTRODUCTION

Silver nanocluster (AgNC) is a class of metallic nanomaterials with a size typically smaller than 2 nm and possesses unique optical and chemical properties (1). It has emerged as a promising candidate for biological labelling and detection (2) due to its higher photostability than organic dye (3), as well as the smaller size and lower toxicity than quantum dots (4). Various methods of synthesizing water-soluble AgNCs have been explored, e.g. radiolytic, chemical reduction and photoreduction (5). A stabilizing scaffold, e.g. dendrimers, polymers and biomolecules, is required to prevent aggregation of the nanoclusters and control their fluorescence properties (6). The use of DNA as a templating scaffold, first reported by Dickson's group in 2004 (7), stands out as a facile synthesis method that can potentially generate a library of fluorescent AgNCs simply by tuning the nucleotide sequence (8,9).

DNA binds to silver (I) ions (Ag^+) primarily at cytosine-rich sites since cytosine is known to have the strongest binding affinity to Ag^+ (10,11). Besides the primary DNA sequence, successful formation of AgNCs also depends on the secondary structure of the DNA template. Brighter AgNCs are obtained from having the cytosine-rich sites in relatively flexible hairpin loops or i-motifs rather than rigid double-stranded DNA (12–14). This suggests that reconfiguration of the DNA structure in presence of the newly formed Ag^0 may be necessary for forming fluorescent AgNC–DNA.

A guanine-assisted turn-on fluorescence format was recently reported by Yeh *et al*. where a 500-fold turn-on fluorescence is achieved upon hybridization to a guanine-rich complementary strand (15). Here, the green-emitting AgNC with extremely low quantum yield ('dark' state) is obtained upon synthesis and then converted to the much brighter red-emitting AgNC ('bright' state) upon hybridization to a guanine-rich strand. The exact mechanism of the guanine-assisted fluorescence is yet to be clearly understood, though it is believed that a combination of physical interaction between N7 of guanine and silver (16), and the electron transfer from guanine to the AgNC, contributes synergistically to the re-organization of the AgNC and results in the strong turn-on fluorescence (15,17). This turn-on system is subsequently applied for the detection of single nucleotide polymorphism (SNP) based on subtle changes in the emission color (18) and in conjunction with rolling circle amplification for the one-pot detection of enzymatic activity (19). However, the questions of how the as-synthesized AgNC–DNA maintains its dark state and the physical process involved in switching the AgNC–DNA to the bright state remain.

In this work, we fill this knowledge gap by presenting the critical role played by the DNA spacer sequence between the two distinct Ag^+-binding cytosine sites in modulating the fluorescence turn-on effect (Figure 1A). The whole Ag^+-binding domain was split into a CCC–spacer–CCCC format instead of viewing it as a single entity, which was the conventional thinking prior to this work. We hypothesized that the spacer spatially separates the two cytosine sites to maintain a quenched dark state, while at the same time physically bridging the two cytosine sites within close proximity to facilitate the guanine-assisted remodeling into a highly fluorescing bright state (Figure 1B). The proposed

*To whom correspondence should be addressed. Tel: +65 6516 1699; Fax: +65 6779 1936; Email: cheyly@nus.edu.sg

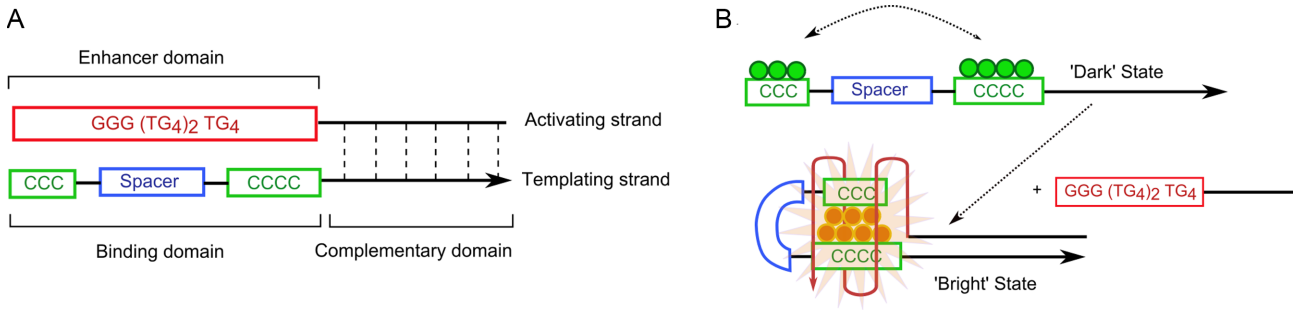

Figure 1. (**A**) The two-strand DNA-templated silver nanocluster (AgNC–DNA) system is characterized by the 'dark' state of the templating strand which turns on to a 'bright' state upon hybridization to a guanine-rich activating strand. The binding domain can be further broken down into a spacer region separating the two Ag^+-binding cytosine sites. (**B**) We propose that the spacer plays an important role in physically separating the two smaller, green-emitting AgNCs formed on the respective cytosine sites to maintain the quenched dark state. The guanine-rich enhancer domain then physically folds the green AgNCs, facilitated by the flexibility of the spacer, into a single larger, highly-fluorescing red-emitting AgNC.

role was found to be universal across spacer sequences of varying lengths and nucleotide compositions. This new insight fills the missing gap in understanding the roles of individual DNA template domains used for AgNC synthesis and contributes a general framework to design template sequences rationally. This understanding culminated in an optimal ATATA spacer design with negligible dark state fluorescence and *ca.* 2440-fold turn-on effect.

MATERIALS AND METHODS

Materials

All DNA oligonucleotides used in this study were purchased from Integrated DNA Technologies (IDT) at the desalted grade. The actual sequences used are shown in Supplementary Table S1. The lyophilized DNA was reconstituted in 1× Tris–EDTA buffer (1× TE, pH 8.0) to give 100 μM stock and stored at 4°C. The following chemicals were used as received: magnesium acetate tetrahydrate ($(CH_3COO)_2Mg{\cdot}4H_2O$, ≥99.0%), silver nitrate ($AgNO_3$, ≥99.0%), sodium borohydride ($NaBH_4$, 99%) were purchased from Sigma Aldrich. 0.1 M phosphate buffer (pH 7.4) was prepared using sodium phosphate dibasic, anhydrous (Na_2HPO_4, ≥99.0%) from Fischer Scientific and sodium phosphate monobasic dehydrate ($NaH_2PO_4{\cdot}2H_2O$, ≥99%) from Kanto Chemical Co. Inc. Milli-Q water (UP) with resistance >18.2 MΩ/cm was used throughout the experiment.

Synthesis of DNA-templated silver nanocluster (AgNC–DNA)

540 μM of $AgNO_3$ was added to 15 μM of templating strand in 20 mM phosphate buffer (pH 7.4). The mixture was vortexed for 5 s and spun down at 14 000 rpm for 30 s. The processed mixture was incubated at 4°C overnight (*ca.* 15 h). 180 μM $NaBH_4$ was freshly prepared in ice-cold Milli-Q water and added immediately to the Ag–DNA mixture. The reaction mixture was vortexed vigorously for 30 s and left undisturbed for 5 h on benchtop. The stated reactant amount refers to the final reaction concentration and the appropriate volume of the respective reactant prepared at a higher stock concentration was added accordingly. The reaction volume was kept constant at 100 μl in this study. All synthesis steps were performed in the dark. The final reactant ratio was DNA:Ag^+:$NaBH_4$ = 1:36:12. The synthesis condition was optimized using the original TTAAT spacer sequence (Supplementary Table S2) and kept constant throughout all analysis in this work.

Hybridization of AgNC–DNA and activating strand

All hybridization reactions were performed within 5–7 h post-synthesis to avoid unnecessary variability in results (explained alongside Figure 8). For all sequence screening analysis, 1 μM of the as-synthesized AgNC–DNA was incubated with 1 μM of activating strand in hybridization buffer of 20 mM phosphate buffer (pH 7.4) and 1 mM magnesium acetate for 1 h at room temperature. For characterizing the limit of detection of the AgNC–DNA system, 100 nM of the as-synthesized AgNC–DNA was titrated with varying concentrations of activating strand in the same hybridization buffer condition.

Optical and mass spectrometry characterization of AgNC–DNA

The absorption spectrum was measured using a UV–vis spectroscopy (Varian Cary 60) and the photoluminescence spectra were measured using a fluorescence spectrophotometer (Varian Cary Eclipse). The analysis volume was kept constant at 1 ml in Hellma semi-micro quartz cuvette. Prior to any photoluminescence measurement, the fluorescent solution was always diluted such that the absorbance remained within 0.02–0.08 to avoid the inner filter effect (20).

The charge and composition of the AgNC–DNA were analyzed using electrospray ionization mass spectrometry (ESI-MS) on a Bruker Compact microTOF-Q. To prepare the sample for MS analysis, the as-synthesized AgNC–DNA was first centrifuged at 14 000 rpm for 30 min to remove any larger particulates. We then desalted the AgNC–DNA using ethanol precipitation. Briefly, the AgNC–DNA supernatant was mixed with 100% ethanol and 0.3 M ammonium acetate (pH 5.2) in a 1:2.5:0.1 ratio (AgNC–DNA: ethanol: ammonium acetate). The mixture was left at 4 °C for 30 min before centrifuging at 14 000 rpm for 15 min.

The AgNC–DNA formed a distinct pellet which was then washed with 70% ethanol, left to dry completely at room temperature, and reconstituted to 100 μM in UP. Before MS analysis, the AgNC–DNA was diluted to 1 μM in 10 mM ammonium acetate solution. The mass spectra were collected on negative ion mode set on a 3.8 kV capillary voltage, 2 bar nebulizer pressure and 150°C dry gas temperature at 120 μl/h flow rate over the range 500–2000 m/z.

Fluorescence measurement of turn-on effect

All turn-on fluorescence study was carried out on a microplate reader (Tecan Infinite M200). The z-position and gain were optimized using the i-control software tool and kept constant throughout the analysis for a given AgNC–DNA concentration. The equipment was pre-equilibrated to the reaction temperature of 25°C prior to all reactions and measurements. All analysis volume was kept constant at 20 μl in Corning NBS 384-well low-volume black polystyrene plate. All experiments were performed in triplicates. Error bars correspond to the sample standard deviation whenever presented.

The extent of turn-on effect was quantitatively represented by the signal-to-noise (S/N) ratio, which can be understood as the ratio of bright state fluorescence to dark state fluorescence. We define signal to be the fluorescence intensity obtained after hybridizing with the activating strand (bright state) and noise to be the fluorescence intensity obtained in absence of the activating strand (dark state). 20 μl hybridization buffer was used as a blank control in all experiments which was subtracted from the respective raw fluorescence measurement data.

All AgNC–DNAs synthesized using different spacer sequences were compared at their individual excitation and emission peaks. First, the hybridized AgNC–DNAs were all excited at 600 nm to determine their emission peaks. The excitation spectrum of individual AgNC–DNAs were then collected at their respective bright state emission peak and the corresponding excitation peak was used to collect the final emission spectrum. The S/N ratio was defined at the respective emission peaks. For characterizing the limit of detection of the ATATA spacer sequence, the excitation and emission wavelengths were fixed at 597 and 656 nm respectively.

RESULTS AND DISCUSSION

Spacer controls the on/off state of AgNC–DNA fluorescence

We first established the critical role of the spacer by comparing two cases: (i) the reported binding domain (15) which contained a TTAAT spacer sequence (**S5**: CCC-TTAAT-CCCC) and (ii) when the spacer was omitted (**S0**: CCC-CCCC). AgNC–DNA was synthesized according to the reported protocol with some modifications (15). Two trends were observed in Figure 2A: the absence of spacer resulted in (i) a rise in the dark state fluorescence (denoted as noise) by *ca.* 5.3-fold and (ii) reduction of the bright state fluorescence (denoted as signal) by *ca.* 60%. This effectively depressed the turn-on effect from 452-fold in **S5** to a mediocre 32.5-fold in **S0**, which confirmed that the spacer sequence played a significant role in controlling the on/off state of the AgNC-DNA fluorescence.

We next varied the nucleotide identity (adenosine, thymine, cytosine and guanine) within the five-nucleotide length spacer. Having cytosine and guanine in the spacer generated appreciable level of dark state fluorescence (Figure 2B). The result was unsurprising as a 12 cytosine binding site is known to fluoresce (21) while guanine is the strongest electron donor among the nucleotides (22). The spacer design space was therefore restricted to adenosine and thymine nucleotides which exhibited relatively quenched dark state. The overall trend was also in line with the reducing power of nucleotides, i.e. G > A > T (cytosine was not considered due to its additional role of binding Ag^+ ions) (22), which supports that electron transfer contributed to the AgNC–DNA fluorescence.

Spacer controls the physical separation between cytosine-rich sites

Since the spacer length controlled the physical separation distance between the two cytosine sites, we varied the spacer length from zero nucleotide (**T0**) to seven nucleotides (**T7**). Only thymine was used for this analysis due to its lowest dark state fluorescence and also to avoid further complications from other nucleotides with higher affinity for Ag^+ ions (23). The dark state fluorescence dropped drastically by *ca.* 80% from the addition of just one thymine (**T1**) and decreased steadily until five thymine were added (**T5**) (Figure 3A).

As the spacer length increased, the bright state fluorescence increased up to an optimal length of three nucleotides (**T3**), beyond which the fluorescence signal dropped steadily and plateaued from five-nucleotide length (**T5**) onward (Figure 3B). This may be understood at the molecular level, where the spacer served as a bridge to hold the two nanoclusters within close proximity for the guanine-rich activating strand to contact and fold them upon each other more easily. Initial increase in the spacer length conferred greater flexibility to facilitate the refolding process. However, when the spacer length and hence flexibility increased further, its bridging effect was less effective, and this increased the difficulty for the activating strand to condense the binding domain. The combined effect on the dark and bright state fluorescence culminated in an optimal separation distance between three to five nucleotides where a drastic turn-on effect, i.e. signal-to-noise (S/N) ratio greater than 1000, was observed (Figure 3B).

Nucleotide composition of spacer influences the AgNC–DNA fluorescence

The nucleotide composition of the spacer could influence the AgNC–DNA fluorescence due to its close proximity to the AgNC, especially the first nucleotide flanking the spacer on either end. Using three-nucleotide spacer length as the simplest model, different nucleotide permutations of thymine and adenosine were designed. For each flanking pairs, *i.e.* A_A, T_A and T_T, we consistently observed that having thymine as the middle nucleotide promoted higher bright state fluorescence with S/N >1000 (Figure 4A). Of

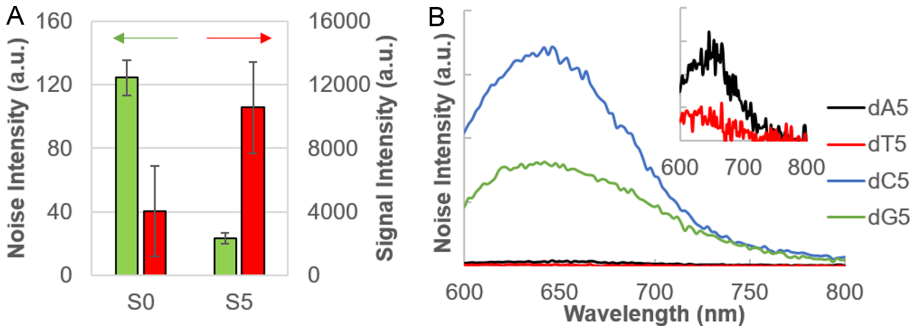

Figure 2. (**A**) Comparison of the dark state (denoted as noise, graph in grey) and bright state (denoted as signal, graph in blue) fluorescence intensity between zero spacer length (**S0**) and five-nucleotide spacer length (**S5**: TTAAT). The full fluorescence spectra are shown in Supplementary Figure S2. (**B**) For a five-nucleotide spacer length, the dark state AgNC fluorescence obtained in absence of the activating strand was ranked as follows: C > G > A > T. Inset: Magnified background fluorescence of fully-A (black) and fully-T (red) spacer.

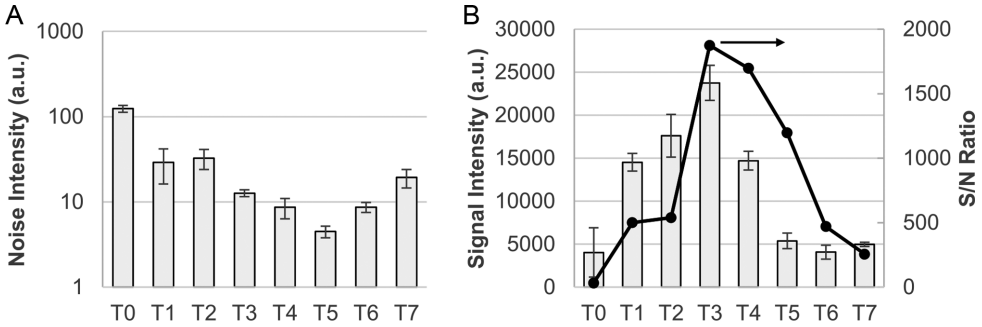

Figure 3. (**A**) The dark state fluorescence (noise) dropped significantly upon the introduction of thymine nucleotides and the system was quenched most effectively from **T3** onward. (**B**) Longer spacer promoted brighter turn-on signals up to an optimal length of three thymine nucleotides (**T3**), beyond which the fluorescence signal dropped steadily. Error bars correspond to the sample standard deviation (n = 3).

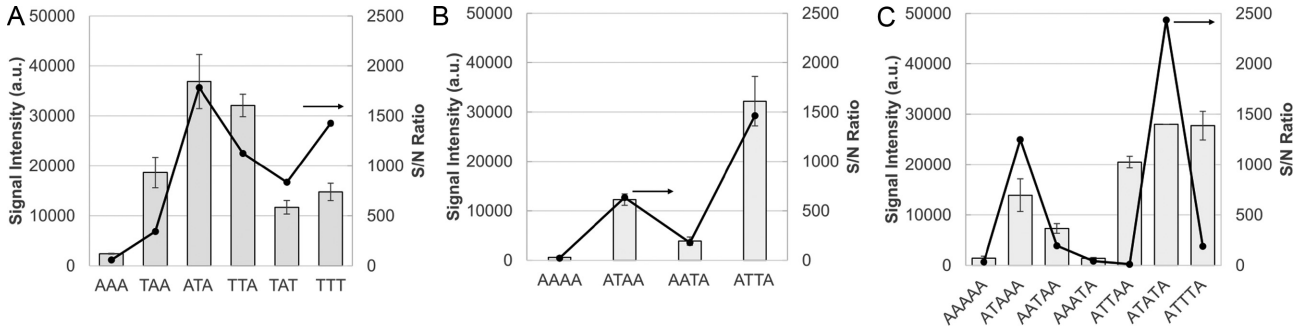

Figure 4. (**A**) Permutations of the immediate nucleotides next to the cytosine-rich regions were tested. ATA sequence generated both the bright state fluorescence (signal) and signal-to-noise (S/N) ratio. (**B**) Keeping adenosine directly next to the cytosine-binding sites, the sequence of the interior nucleotides was varied for a four-nucleotide spacer length. (**C**) Further extension of the spacer length to five nucleotides yielded ATATA spacer sequence with the highest S/N ratio of 2440. Error bars correspond to the sample standard deviation ($n = 3$).

the three cases, ATA generated the brightest signal and highest S/N ratio. This suggests that having an adenosine pair as the flanking nucleotide facilitated the turn-on process. One reason could be that adenosine is the stronger electron donor of the two and contributed more significantly toward signal enhancement after the activating strand reorganized the AgNC into the bright state.

After retaining the adenosine pair as the flanking nucleotide, we investigated other nucleotide permutations for four- and five-nucleotide spacer lengths to determine the positional effect. Comparing ATAA vs AATA (Figure 4B), and ATAAA versus AATAA versus AAATA (Figure 4C), having thymine nearer the 5′-end was advantageous for generating strong turn-on signal. Also, increasing proportion of thymine nucleotides resulted in stronger turn-on signal. However, having contiguous thymine increased the dark state fluorescence (Figure 5). The poor turn-on effect was similarly observed when contiguous adenosine was involved, *e.g.* AAA and TAA (Figure 4A). Generally, we recommend having adenosine and thymine as close to equal proportion as possible in the spacer while avoiding contiguous stretch of either nucleotide.

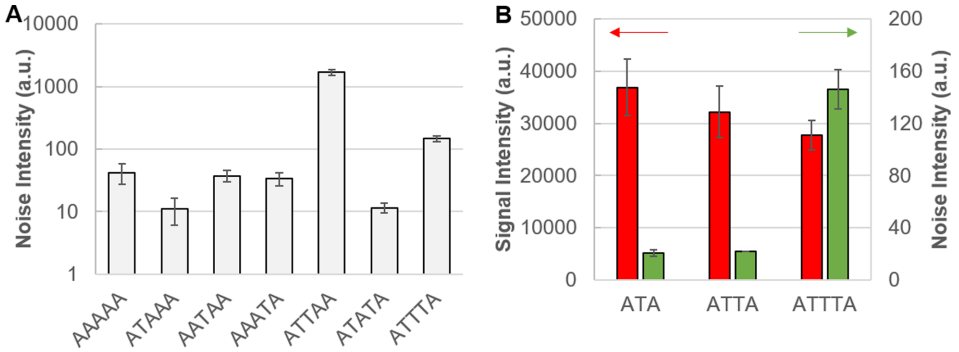

Figure 5. (**A**) The dark state fluorescence was relatively higher when contiguous stretches of thymine or adenosine were present. The highest noise intensity was obtained for ATTAA where both contiguous thymine and adenosine were present. Note that the y-axis was shown in log scale to represent varying magnitudes of fluorescence clearly. (**B**) Keeping adenosine as the flanking nucleotides, the spacer length was increased by adding more thymine nucleotides. The activated signal decreased as the spacer length increased while the dark state fluorescence increased exponentially as the percentage of contiguous thymine increased. 1 μM of AgNC–DNA was hybridized with 1 μM of activating strand. Error bars correspond to the sample standard deviation ($n = 3$).

Proposed mechanism for spacer-modulated turn-on fluorescence

The turn-on effect arising from a quenched dark state and guanine-activated bright state was consistently observed across all spacer sequences tested (Figure 6). This further validated the role of the spacer within the binding domain in modulating the extent of turn-on fluorescence. It was reported that DNA-stabilized AgNC typically consists of four or six silver atoms (Ag^0) which correspond to two magic colors of green and red respectively (24). In the single-stranded templating strand, two distinct cytosine sites ('CCC' and 'CCCC') are present. Given that the dark state AgNC is predominantly green-emitting, it is possible that two distinct 'magic' clusters of three to four Ag^0 are formed instead of six or more Ag^0 as expected from a seven-cytosine sequence. The physical presence of the spacer separates the two cytosine sites to maintain the AgNC in the smaller, green-emitting form (Figure 1B). The guanine-rich activating strand then comes into physical contact with the two dark nanoclusters, held together by the spacer, and folds them upon themselves for re-organization into a single *ca.* six-atom red-emitter.

Based on the mass spectrum obtained from ESI-MS analysis (Supplementary Figure S3), we calculated the number of neutral Ag^0 atoms and positively-charged Ag^+ atoms (refer to SI for detailed method), and found that majority of the DNA sequences used in this study generated AgNCs with six neutral Ag^0 atom and one or two Ag^0 variation for some strands (Supplementary Table S3), which was in line with the magic number expected of AgNC–DNA (24). The number of Ag^+ atoms was greater than Ag^0 atoms, in line with existing knowledge that a highly positive cluster core is essential for holding the structure of AgNC–DNA together (25). There was no correlation between the number of Ag^0 atoms and the AgNC–DNA brightness, extent of turn-on signal or emission wavelength. These observations did not fit into the existing rod shape model wherein having more neutral Ag^0 atoms should increase the AgNC rod length and hence the extent of emission red-shift (26,27). Perhaps the rod shape model does not apply generally across all AgNC–DNAs and alternative models such as the octahedral geometry have been proposed recently (28). We were unable to segregate the species responsible for 'dark' and 'bright' state as all Ag species were present on the single DNA strand, though with different molecular configuration which could not be distinguished by ESI-MS.

High quality AgNC–DNA with drastic turn-on effect

Among the spacer sequences explored in this work, ATATA performed the best with the highest S/N ratio of 2440 (Figure 4C). This turn-on effect was 5-fold higher than that reported by Yeh's group (15). Even though the absolute turn-on signal was slightly weaker for the longer five-nucleotide spacer length compared to the shorter three-nucleotide cases, the ATATA spacer sequence stood out for its negligible dark state fluorescence which resulted in a drastic turn-on effect.

The strong turn-on effect of the AgNC synthesized using DNA template with the ATATA spacer sequence could be attributed to three reasons (Figure 7A). First, the spacer design was effective in separating and quenching the two nanocluster sites which minimized the unassisted formation of bright state AgNC. Next, the bright state emission was in the far-red region ($\lambda_{em} = 656$ nm) with an excitation peak at 597 nm which effectively minimized spectral cross-talk with the dark state species ($\lambda_{ex} = 500$ nm, $\lambda_{em} = 563$ nm) (Figure 7B). Lastly, the optimized sequence generated a single homogeneous emitter (Supplementary Figure S4) with a narrow full-width half maximum (FWHM) of 72 nm which contributed to the reproducibility of the fluorescence signal (Figure 7B). This narrow FWHM was comparable to purified AgNC–DNA containing only a single AgNC emitter with a reported FWHM of *ca.* 90 nm (14,26).

Next, we characterized the kinetics of AgNC–DNA formation and guanine-activated turn-on effect by following the changes in the UV–vis absorption spectrum using the ATATA spacer strand. Within the first minute after reduction with $NaBH_4$, a broad absorption spectrum formed between the 350 and 500 nm (Figure 8A). We visually observed a dark yellow solution which corresponded to the instant nucleation of small Ag particles in solution arising from the rapid reduction reaction (29). In the next minute, a sharp peak formed at *ca.* 363 nm with a shoulder in 400 nm range. This sharp peak gradually declined within the

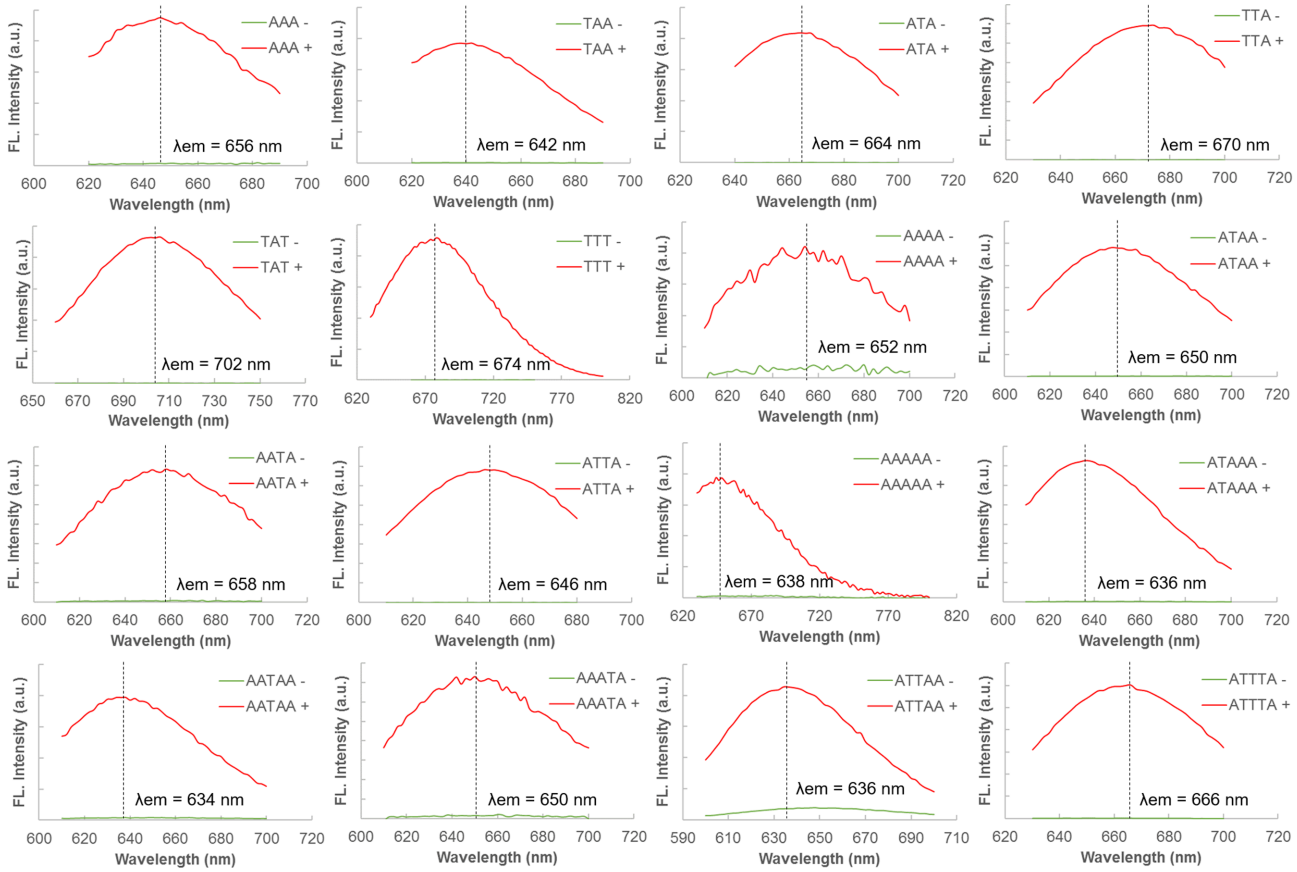

Figure 6. Emission spectra of AgNCs templated by DNA with different spacer sequences (Supplementary Table S1). The normalized emission spectra of 1 μM as-synthesized AgNC–DNAs (dark state) were presented as green solid lines while those reacted with 1 μM of activating strand (bright state) were presented as red solid lines. The dark state fluorescence intensity was signficantly lower than the bright state fluorescence intensity across all spacer sequences, albeit of varying magnitude. This supported our concept of viewing the spacer as a standalone entity to modulate the fluorescence turn-on effect.

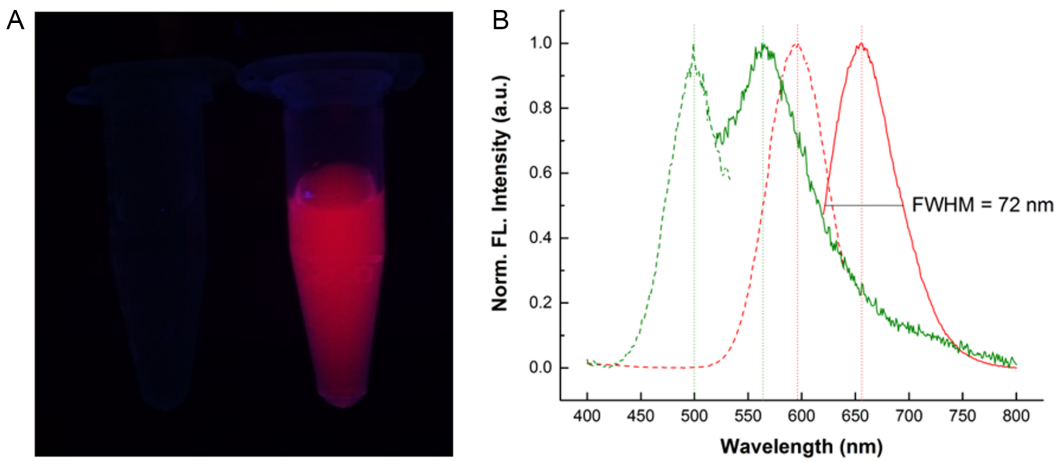

Figure 7. (**A**) Digicam image of (left) 1 μM of the as-synthesized AgNC–DNA and (right) when mixed with 1 μM of activating strand. (**B**) Normalized excitation (dotted lines) and emission (solid lines) spectra of the dark (green) and bright (red) state. The emission spectrum of the bright state AgNC-DNA exhibited a narrow full-width half maximum (FWHM) of 72 nm.

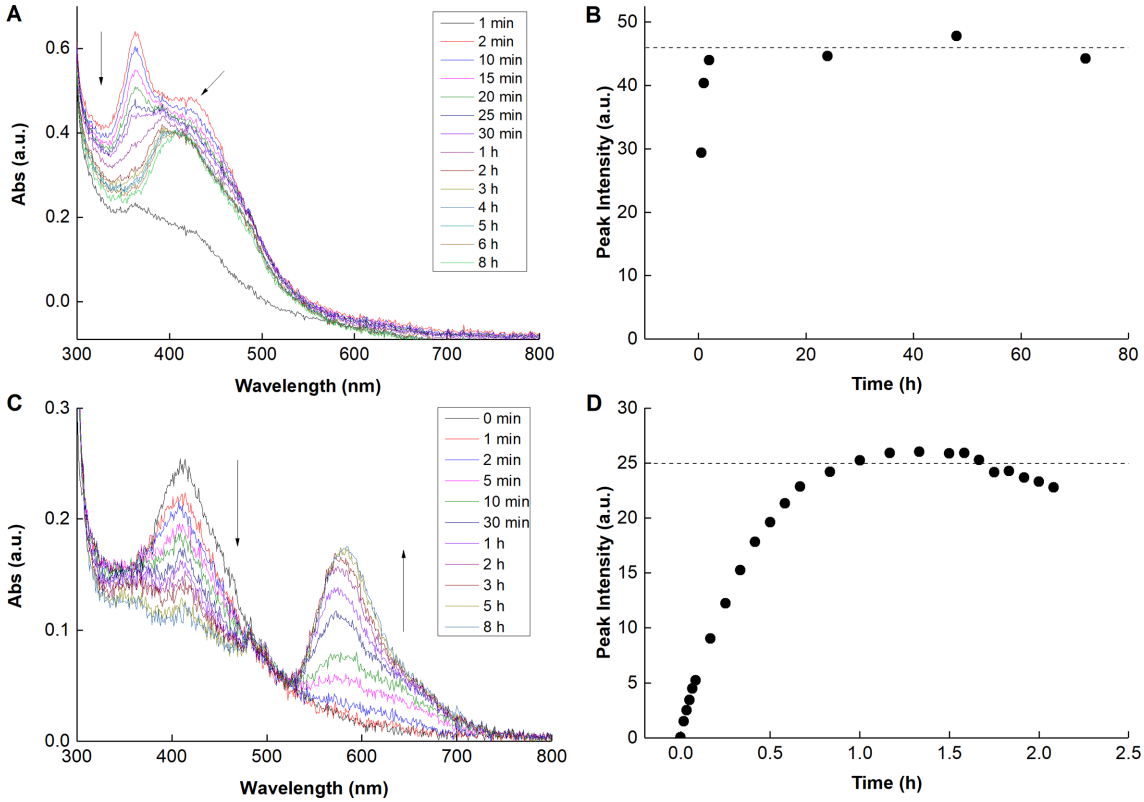

Figure 8. (**A**) Kinetics of the formation of AgNC–DNA upon addition of NaBH4 ($t = 0$ min) based on UV–vis absorption measurement over time. (**B**) The stability of AgNC–DNA formed was confirmed by hybridizing with the guanine-activating strand and measuring its fluorescence emission at selected time points. (**C**) Kinetics of the molecular reconfiguration of AgNC–DNA from dark (409 nm) to bright (589 nm) state upon hybridization with the guanine-activating strand based on UV–vis absorption measurement over time. (**D**) The activation of the bright state fluorescence reached equilibrium *ca.* 1 h post-hybridization. All characterization works presented were performed on the ATATA spacer sequence. Dotted lines were included in (B) and (D) as a guide to the equilibrium state.

next 30 min while the original shoulder shaped to become the new absorption peak at 409 nm. This represented the growth stage of AgNC formation where the Ag^0 nuclei coalesce into larger clusters, which in this case, represented the dark state AgNC (30). The number of Ag atoms per species was limited by the DNA template which passivated the surface of the newly-formed AgNC–DNA. The absorption spectrum stabilized from 2 h post-synthesis onward. The stability of the AgNC–DNA over time was maintained for at least three days, as confirmed by hybridizing with the guanine-rich activating strand and measuring their fluorescence emissions at selected time points (Figure 8B). We should point out that the AgNC–DNA stability differed according to the DNA template sequence and a window period of 5–7 h post-synthesis was optimal to obtain stable peak intensity across all sequences (data not shown).

Upon hybridization with the guanine-rich strand, we observed a decline in the absorption peak at 409 nm and an increase in the 589 nm peak (Figure 8C). This corresponded to an increase in the fluorescence intensity of the red-emitting bright state AgNC (Figure 8D). We deduced that the 409 and 598 nm absorption peak corresponded to the dark and bright state AgNC respectively, and that the molecular configuration process was mediated by the guanine-rich strand. Also, the bright state emission reached equilibrium *ca.* 1 h post-synthesis (Figure 8D).

Demonstration of optimized template sequence for DNA detection in picomolar range

The final optimized design was then tested for its performance as a AgNC–DNA detection probe. We titrated 100 nM of the as-synthesized AgNC–DNA with varying concentrations of the activating strand. Strong turn-on fluorescence was observed within an hour of hybridization (Figure 9A). There was a clear linear relationship ($R^2 = 0.980$) between the bright state fluorescence intensity and concentration of the activating strand, which rendered this design a potential tool for target quantification (Figure 9B). Due to the lack of dark state fluorescence, a good limit of detection of 87 pM (defined as three standard deviations from the mean of the blank measurement) was obtained. This was noticeably lower than other similar guanine-activated AgNC–DNA systems where the LODs are typically in the nanomolar range (31–33).

Metallic nanocluster has great potential for biomedical applications, e.g. as imaging probes and for photodynamic therapy (34), and as an analytical tool (35,36). The use of DNA template has the advantage of achieving specific target recognition through the direct incorporation of complementary DNA or aptamer sequences without the need for post-synthesis functionalization (37–40). There has been increased understanding on how the structure of AgNC

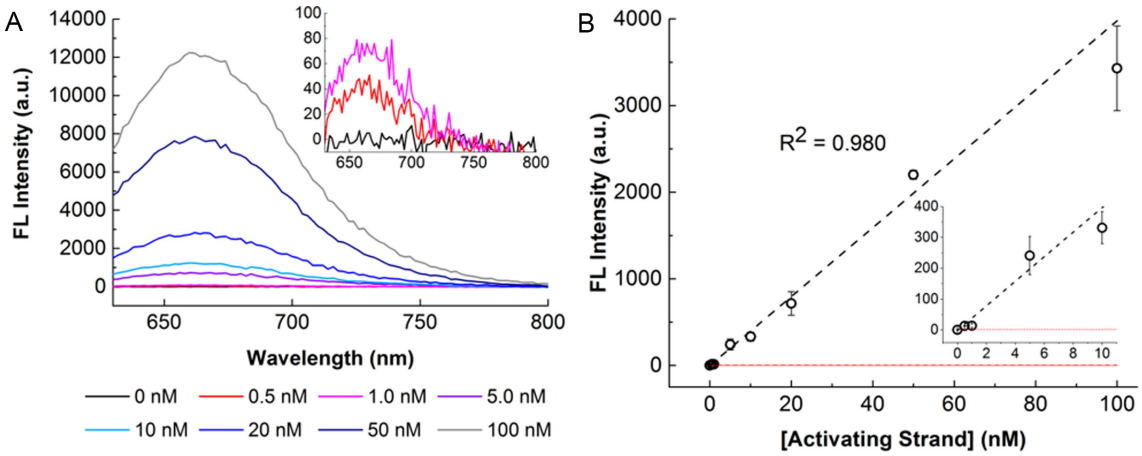

Figure 9. (**A**) Fluorescence (FL) intensity of 100 nM AgNC-DNA with the optimized spacer sequence (ATATA) when titrated with different concentrations of activating strand (0–100 nM). Inset: Magnified view for 0 nM (black), 0.5 nM (red) and 1.0 nM (pink) of activating strand. Notably, the dark state exhibited negligible amount of fluorescence. (**B**) There was a clear dosage-dependence between the AgNC-DNA fluorescence intensity and concentration of activating strand. The solid red line corresponds to the mean background noise while the dotted red line corresponds to 3 standard deviations from the mean noise level. Error bars correspond to the sample standard deviation ($n = 3$).

correlates to its fluorescence properties (41–45); though for AgNC–DNA to truly take off as a toolbox for biomedical applications, the next technical hurdle is to generate DNA sequences for templating AgNC–DNA with good stability particularly in a chloride-rich environment (46). Some strategies were previously proposed to enhance the stability of AgNC–DNA, e.g. using triplex DNA (47) and specific sequence design (48). However, a concrete understanding of the mechanism of stabilization or empirical guidelines on the DNA sequence design for generating stable, brightly fluorescing AgNC is still lacking. We are currently investigating the sequence-function relationship between the DNA sequences and the stability of the AgNC fluorescence in order to enhance our current design framework for generating bright and stable AgNC–DNA probes in the near future.

CONCLUSION

In conclusion, we established the role of the spacer sequence in the AgNC binding domain to spatially separate the two smaller, dark state AgNCs in the templating strand while bridging them sufficiently close for refolding by the guanine-rich activating strand into the bright state form. As such, the AgNC–DNA is fully defined in terms of template sequence and can be designed rationally for improved photophysical properties and specific applications. An optimal spacer length of three to five nucleotides was a good balance point. We recommend using only adenosine and thymine in the spacer to achieve a good turn-on effect. Contiguous stretches of either nucleotide should be avoided as they often led to significant level of dark state fluorescence. Based on these guidelines, we identified ATATA as the best spacer sequence with a drastic turn-on effect of 2440-fold which is the highest reported to date (five times that of the highest factor reported). Due to its highly quenched dark state, strong turn-on effect could still be observed even at picomolar concentration of the activating strand. More template sequences can be evolved from this general framework to generate better AgNC-DNA systems, e.g. with stronger fluorescence signal or improved photostability.

SUPPLEMENTARY DATA

Supplementary Data are available at NAR Online.

FUNDING

Singapore Ministry of Education Academic Research Fund Tier 1. Funding for open access charge: Singapore Ministry of Education Academic Research Fund Tier 1; National University of Singapore and Ministry of Education for the President Graduate Fellowship (to Y.S.A.).
Conflict of interest statement. None declared.

REFERENCES

1. Lu,Y. and Chen,W. (2012) Sub-nanometre sized metal clusters: from synthetic challenges to the unique property discoveries. *Chem. Soc. Rev.*, **41**, 3594–3623.
2. Choi,S., Dickson,R.M. and Yu,J. (2012) Developing luminescent silver nanodots for biological applications. *Chem. Soc. Rev.*, **41**, 1867–1891.
3. Vosch,T., Antoku,Y., Hsiang,J.-C., Richards,C.I., Gonzalez,J.I. and Dickson,R.M. (2007) Strongly emissive individual DNA-encapsulated Ag nanoclusters as single-molecule fluorophores. *Proc. Natl. Acad. Sci. U.S.A.*, **104**, 12616–12621.
4. Shang,L., Dong,S. and Nienhaus,G.U. (2011) Ultra-small fluorescent metal nanoclusters: synthesis and biological applications. *Nano Today*, **6**, 401–418.
5. Xu,H. and Suslick,K.S. (2010) Water-soluble fluorescent silver nanoclusters. *Adv. Mater.*, **22**, 1078–1082.
6. Diez,I. and Ras,R.H.A. (2011) Fluorescent silver nanoclusters. *Nanoscale*, **3**, 1963–1970.
7. Petty,J.T., Zheng,J., Hud,N.V. and Dickson,R.M. (2004) DNA-templated Ag nanocluster formation. *J. Am. Chem. Soc.*, **126**, 5207–5212.
8. Sharma,J., Yeh,H.-C., Yoo,H., Werner,J.H. and Martinez,J.S. (2010) A complementary palette of fluorescent silver nanoclusters. *Chem. Commun.*, **46**, 3280–3282.
9. Richards,C.I., Choi,S., Hsiang,J.-C., Antoku,Y., Vosch,T., Bongiorno,A., Tzeng,Y.-L. and Dickson,R.M. (2008)

Oligonucleotide-stabilized Ag nanocluster fluorophores. *J. Am. Chem. Soc.*, **130**, 5038–5039.
10. Ono,A., Cao,S., Togashi,H., Tashiro,M., Fujimoto,T., Machinami,T., Oda,S., Miyake,Y., Okamoto,I. and Tanaka,Y. (2008) Specific interactions between silver(i) ions and cytosine-cytosine pairs in DNA duplexes. *Chem. Commun.*, 4825–4827.
11. Yang,X., Gan,L., Han,L., Wang,E. and Wang,J. (2013) High-yield synthesis of silver nanoclusters protected by DNA monomers and DFT prediction of their photoluminescence properties. *Angew. Chem. Int. Ed.*, **52**, 2022–2026.
12. Sengupta,B., Springer,K., Buckman,J.G., Story,S.P., Abe,O.H., Hasan,Z.W., Prudowsky,Z.D., Rudisill,S.E., Degtyareva,N.N. and Petty,J.T. (2009) DNA templates for fluorescent silver clusters and I-motif folding. *J. Phys. Chem. C*, **113**, 19518–19524.
13. Gwinn,E.G., O'Neill,P., Guerrero,A.J., Bouwmeester,D. and Fygenson,D.K. (2008) Sequence-dependent fluorescence of DNA-hosted silver nanoclusters. *Adv. Mater.*, **20**, 279–283.
14. Del Bonis-O'Donnell,J.T., Pennathur,S. and Fygenson,D.K. (2016) Changes in spectra and conformation of hairpin DNA-stabilized silver nanoclusters induced by stem sequence perturbations. *Langmuir*, **32**, 569–576.
15. Yeh,H.-C., Sharma,J., Han,J.J., Martinez,J.S. and Werner,J.H. (2010) A DNA−silver nanocluster probe that fluoresces upon hybridization. *Nano Lett.*, **10**, 3106–3110.
16. Arakawa,H., Neault,J.F. and Tajmir-Riahi,H.A. (2001) Silver(I) complexes with DNA and RNA studied by fourier transform infrared spectroscopy and capillary electrophoresis. *Biophys. J.*, **81**, 1580–1587.
17. Sylwia,W., Kiyoshi,M., Moin,A. and Juewen,L. (2014) Towards understanding of poly-guanine activated fluorescent silver nanoclusters. *Nanotechnology*, **25**, 155501.
18. Yeh,H.-C., Sharma,J., Shih,I.-M., Vu,D.M., Martinez,J.S. and Werner,J.H. (2012) A fluorescence light-up Ag nanocluster probe that discriminates single-nucleotide variants by emission color. *J. Am. Chem. Soc.*, **134**, 11550–11558.
19. Juul,S., Obliosca,J.M., Liu,C., Liu,Y.-L., Chen,Y.-A., Imphean,D.M., Knudsen,B.R., Ho,Y.-P., Leong,K.W. and Yeh,H.-C. (2015) NanoCluster Beacons as reporter probes in rolling circle enhanced enzyme activity detection. *Nanoscale*, **7**, 8332–8337.
20. Ang,Y.S. and Yung,L.Y.L. (2014) Toehold-mediated internal control to probe the near-field interaction between the metallic nanoparticle and the fluorophore. *Nanoscale*, **6**, 12515–12523.
21. Ritchie,C.M., Johnsen,K.R., Kiser,J.R., Antoku,Y., Dickson,R.M. and Petty,J.T. (2007) Ag nanocluster formation using a cytosine oligonucleotide template. *J. Phys. Chem. C*, **111**, 175–181.
22. Crespo-Hernández,C.E., Close,D.M., Gorb,L. and Leszczynski,J. (2007) Determination of redox potentials for the watson−crick base pairs, dna nucleosides, and relevant nucleoside analogues. *J. Phys. Chem. B*, **111**, 5386–5395.
23. Soto-Verdugo,V., Metiu,H. and Gwinn,E. (2010) The properties of small Ag clusters bound to DNA bases. *J. Chem. Phys.*, **132**, 195102.
24. Copp,S.M., Schultz,D., Swasey,S., Pavlovich,J., Debord,M., Chiu,A., Olsson,K. and Gwinn,E. (2014) Magic numbers in DNA-stabilized fluorescent silver clusters lead to magic colors. *J. Phys. Chem. Lett.*, **5**, 959–963.
25. Koszinowski,K. and Ballweg,K. (2010) A highly charged Ag64+ core in a DNA-encapsulated silver nanocluster. *Chem. Eur. J.*, **16**, 3285–3290.
26. Schultz,D. and Gwinn,E.G. (2012) Silver atom and strand numbers in fluorescent and dark Ag:DNAs. *Chem. Commun.*, **48**, 5748–5750.
27. Schultz,D., Gardner,K., Oemrawsingh,S.S.R., Markešević,N., Olsson,K., Debord,M., Bouwmeester,D. and Gwinn,E. (2013) Evidence for rod-shaped DNA-stabilized silver nanocluster emitters. *Adv. Mater.*, **25**, 2797–2803.
28. Petty,J.T., Sergev,O.O., Ganguly,M., Rankine,I.J., Chevrier,D.M. and Zhang,P. (2016) A segregated, partially oxidized, and compact Ag10 cluster within an encapsulating DNA host. *J. Am. Chem. Soc.*, **138**, 3469–3477.
29. Agnihotri,S., Mukherji,S. and Mukherji,S. (2014) Size-controlled silver nanoparticles synthesized over the range 5–100 nm using the same protocol and their antibacterial efficacy. *RSC Adv.*, **4**, 3974–3983.
30. Thanh,N.T.K., Maclean,N. and Mahiddine,S. (2014) Mechanisms of nucleation and growth of nanoparticles in solution. *Chem. Rev.*, **114**, 7610–7630.
31. Zhang,L., Zhu,J., Zhou,Z., Guo,S., Li,J., Dong,S. and Wang,E. (2013) A new approach to light up DNA/Ag nanocluster-based beacons for bioanalysis. *Chem. Sci.*, **4**, 4004–4010.
32. Zhang,Y., Zhu,C., Zhang,L., Tan,C., Yang,J., Chen,B., Wang,L. and Zhang,H. (2015) DNA-templated silver nanoclusters for multiplexed fluorescent DNA detection. *Small*, **11**, 1385–1389.
33. Feng,L., Liu,J., Zhang,S.C. and Zhang,X.R. (2015) Label-free DNA detection based on a DNA-silver nanocluster pair. *Anal. Methods*, **7**, 5689–5694.
34. Song,X.-R., Goswami,N., Yang,H.-H. and Xie,J. (2016) Functionalization of metal nanoclusters for biomedical applications. *Analyst*, **141**, 3126–3140.
35. Ran,X., Wang,Z., Zhang,Z., Pu,F., Ren,J. and Qu,X. (2016) Nucleic-acid-programmed Ag-nanoclusters as a generic platform for visualization of latent fingerprints and exogenous substances. *Chem. Commun.*, **52**, 557–560.
36. Yang,S.W. and Vosch,T. (2011) Rapid detection of MicroRNA by a silver nanocluster DNA probe. *Anal. Chem.*, **83**, 6935–6939.
37. Yin,J., He,X., Wang,K., Qing,Z., Wu,X., Shi,H. and Yang,X. (2012) One-step engineering of silver nanoclusters-aptamer assemblies as luminescent labels to target tumor cells. *Nanoscale*, **4**, 110–112.
38. Li,J., Zhong,X., Cheng,F., Zhang,J.-R., Jiang,L.-P. and Zhu,J.-J. (2012) One-pot synthesis of aptamer-functionalized silver nanoclusters for cell-type-specific imaging. *Anal. Chem.*, **84**, 4140–4146.
39. Yin,J., He,X., Wang,K., Xu,F., Shangguan,J., He,D. and Shi,H. (2013) Label-free and turn-on aptamer strategy for cancer cells detection based on a DNA–silver nanocluster fluorescence upon recognition-induced hybridization. *Anal. Chem.*, **85**, 12011–12019.
40. Li,J., Zhong,X., Zhang,H., Le,X.C. and Zhu,J.-J. (2012) Binding-induced fluorescence turn-on assay using aptamer-functionalized silver nanocluster DNA probes. *Anal. Chem.*, **84**, 5170–5174.
41. New,S.Y., Lee,S.T. and Su,X.D. (2016) DNA-templated silver nanoclusters: structural correlation and fluorescence modulation. *Nanoscale*, **8**, 17729–17746.
42. Petty,J.T., Giri,B., Miller,I.C., Nicholson,D.A., Sergev,O.O., Banks,T.M. and Story,S.P. (2013) Silver clusters as both chromophoric reporters and DNA ligands. *Anal. Chem.*, **85**, 2183–2190.
43. Petty,J.T., Sergev,O.O., Kantor,A.G., Rankine,I.J., Ganguly,M., David,F.D., Wheeler,S.K. and Wheeler,J.F. (2015) Ten-atom silver cluster signaling and tempering DNA hybridization. *Anal. Chem.*, **87**, 5302–5309.
44. Ganguly,M., Bradsher,C., Goodwin,P. and Petty,J.T. (2015) DNA-directed fluorescence switching of silver clusters. *J. Phys. Chem. C*, **119**, 27829–27837.
45. Lin,R., Tao,G., Chen,Y., Chen,M., Liu,F. and Li,N. (2017) Constructing a robust fluorescent DNA-stabilized silver nanocluster probe module by attaching a duplex moiety. *Chem. Eur. J.*, **23**, 10893–10900.
46. Pratik,S., Seok Keun,C., Peter Waaben,T., Yong-Joo,B., Jong Cheol,A., Suk Won,C., Andreas,R.-L. and Seong Wook,Y. (2014) Effect of salts, solvents and buffer on miRNA detection using DNA silver nanocluster (DNA/AgNCs) probes. *Nanotechnology*, **25**, 045101.
47. Feng,L., Huang,Z., Ren,J. and Qu,X. (2012) Toward site-specific, homogeneous and highly stable fluorescent silver nanoclusters fabrication on triplex DNA scaffolds. *Nucleic. Acids. Res.*, **40**, e122.
48. Yuan,Z., Chen,Y.-C., Li,H.-W. and Chang,H.-T. (2014) Fluorescent silver nanoclusters stabilized by DNA scaffolds. *Chem. Commun.*, **50**, 9800–9815.